Indones. J. Chem., 2021, 21 (6), 1471 - 1483

1471

Modification of Fishbone-Based Hydroxyapatite with MnFe$_2$O$_4$ for Efficient Adsorption of Cd(II) and Ni(II) from Aqueous Solution

Poedji Loekitowati Hariani[1,2], Addy Rachmat[1,2*], Muhammad Said[1,2], and Salni Salni[3]

[1]*Department of Chemistry, Faculty of Mathematics and Natural Sciences, Universitas Sriwijaya,*
Jl. Palembang Prabumulih Km. 32, Ogan Ilir 30662, Indonesia

[2]*Research Centre of Advanced Material and Nanocomposite, Faculty of Mathematics and Natural Sciences, Universitas Sriwijaya,*
Jl. Palembang Prabumulih Km. 32, Ogan Ilir 30662, Indonesia

[3]*Department of Biology, Faculty of Mathematics and Natural Sciences, Jl. Palembang Prabumulih Km. 32,*
Ogan Ilir 30662, Indonesia

Abstract: *Due to their toxicity, Cd(II) and Ni(II) ions in the environment are severe. The hydroxyapatite composite was improved with magnetic MnFe$_2$O$_4$ to remove Cd(II) and Ni(II) ions from an aqueous solution. Hydroxyapatite was extracted from Snakehead* (Channa striata) *fish bones via alkaline-heat treatment. The hydroxyapatite/MnFe$_2$O$_4$ composite performance was analyzed through XRD, FTIR, SEM-EDS, BET analysis, and VSM, and the results reveal that the hydroxyapatite/MnFe$_2$O$_4$ composite shows good magnetic properties of 21.95 emu/g. The kinetics evaluation confirmed that the pseudo-second-order kinetics model was more suitable to describe the adsorption of Cd(II) and Ni(II) ions by hydroxyapatite/MnFe$_2$O$_4$ composite from the solution. The Langmuir isotherm model was suitable to describe the adsorption process of the Cd(II) and Ni(II) ions, where the adsorption capacities for Cd(II) and Ni(II) are 54.3 and 47.4 mg/g, respectively. Desorption of Cd(II) and Ni(II) ions from hydroxyapatite/MnFe$_2$O$_4$ composite using NaCl as the eluent was more effective than EDTA. The findings of this study indicate that hydroxyapatite/MnFe$_2$O$_4$ can reduce Cd(II) and Ni(II) ions in wastewater so that it can recover natural resources.*

Keywords: *hydroxyapatite/MnFe$_2$O$_4$ composite; adsorption; Cd(II); Ni(II); desorption*

■ INTRODUCTION

Wastewater discharged from industrial activities is one of the environmental issues; hence its treatment is a paramount concern. Wastewater containing heavy metals is a notable concern due to its toxicity and ease of accumulating in the food chain. It is harmful to human life and the environment as well [1-2]. Some industries generate wastes containing heavy metals such as mining, ceramics, pesticides, smelting, and steel [2-3]. Cadmium poisoning causes a detrimental effect on kidneys, lungs, hypertension, liver, in addition to the teratogenic impacts [4]. Exposure to nickel can trigger kidney, lung, and cardiovascular disorders [5]. It also causes headaches, dermatitis, and respiratory disorders [6-7]. According to

the World Health Organization, the maximum thresholds of Cd and Ni in drinking water are 0.003 mg/L and 0.07 mg/L, respectively.

Various methods have been developed to reduce the concentration of heavy metals in water, such as adsorption [3], membrane processes [8], bioremediation [9], reverse osmosis [10], and ion exchange [11]. Among these methods, adsorption is the most commonly used due to ease of operation, flexible design, and non-toxic properties [1-2]. In addition, using low-cost adsorbents makes the adsorption method even economical. These low-cost adsorbents can be obtained from various sources such as calcium alginate/spent coffee grounds composite beads [3], expanded perlite [12],

hydroxyapatite [13], green logan hull [14], and succinylated hay [15].

Hydroxyapatite ($Ca_{10}(PO_4)_6(OH)_2$) is widely used as catalyst, fertilizer, and adsorbent in wastewater treatment, chromatography, bone, and dental implants [16-17]. Hydroxyapatite had been used to adsorb various metal cations such as Cd(II), Pb(II), and Ni(II) [13]. Hydroxyapatite prepared from different precursors was also reported for Pb(II) [18-19]. Some natural materials containing calcium, such as fishbone, can be used for making hydroxyapatite. It is estimated that 30–40% of total fish production leaves solid waste [20]. Using fishbones as a source of hydroxyapatite provide advantages due to its cheapness, abundance in nature, and its capability of reducing solid waste. Several types of fish as a source of hydroxyapatite include Gray triggerfish skin and Black scabbardfish [21], *Scomberomorus commerson* and *Chirocentrus nudus* [22], and Snakehead fish [23]. Indonesia's people widely consume snakehead fish. Therefore, snakehead fish bones availability provides a potential source of hydroxyapatite. Hydroxyapatite from snakehead fish bones reported possess antibacterial activity against *Escherichia coli* and *Staphylococcus aureus* [24].

Several authors developed hydroxyapatite combined materials to increase the effectiveness of adsorption in the form of hydroxyapatite-rice husk [17], hydroxyapatite-magnetite [25], hydroxyapatite-Fe_3O_4-β-cyclodextrin [26], and hydroxyapatite-chitosan [27]. Adsorbents with magnetic properties recently have been developed. After the adsorption process, the adsorbent can be separated rapidly and effectively using an external magnet without the filtration process [28]. Activated carbon-$MnFe_2O_4$ showed a large adsorption capacity to the removal of As(II) and As(V) [29]. On the other hand, graphite modified with $MnFe_2O_4$ is effective in the removal of Pb(II) and Ni(II) [30].

In this study, hydroxyapatite was extracted from snakehead fish bones by alkaline-heat treatment. The resulting materials were incorporated with $MnFe_2O_4$ by using the co-precipitation method. $MnFe_2O_4$ is a ferrite compound with a large surface area, large magnetic properties, and excellent chemical stability [28]. The composite was used to remove Cd(II) and Ni(II) ions. The adsorption process is carried out in batch mode. Desorption and regeneration were also carried out to evaluate economic interest.

■ EXPERIMENTAL SECTION

Materials

The chemicals used were HCl, NaOH, $MnCl_2 \cdot 4H_2O$, $FeCl_3 \cdot 6H_2O$, $CdCl_2$, $NiCl_2 \cdot 6H_2O$, KNO_3, NaCl, EDTA ($C_{10}H_{14}N_2Na_2O_8 \cdot 2H_2O$), all purchased from Merck, Germany and used without further purification. Snakehead fishbone was obtained from the local market in the city of Palembang, South Sumatra, Indonesia.

Instrumentation

The diffractogram pattern was measured using X-ray diffraction (XRD Shimadzu XD-610) with Cu-Kα radiation of 1.54 Å, and the intensity was scanned at 2θ angle from 10° to 80° to observe the crystalline structure. The functional groups were determined using a Fourier transform infrared spectroscopy (FTIR Thermo Fisher Scientific) at 400–4000 cm⁻¹. Surface area calculated according to data recorded by ASAP 2020 analyzer. A vibrating sample magnetometer (VSM Lakeshore 74004) was used to measure saturation magnetization, while a scanning electron microscope/energy-dispersive X-ray spectroscopy (SEM-EDX Shimadzu AA-700) aimed to observe surface morphology and determine the elemental composition. Cd(II) and Ni(II) ions concentration using atomic absorption spectroscopy (AAS Shimadzu AA 7000).

Procedure

Extraction of hydroxyapatite

The extraction of hydroxyapatite was conducted using alkali-heat treatment. Snakehead fish bones prior extraction process were screened from impurities and washed using distilled water. A hundred grams of the bones were placed in the oven for 60 min at 105 °C. The bones were crushed by fast milling tool to obtain 200 mesh particle size. The powder was then washed using 0.1 N HCl to remove the protein, followed by distilled water several times. Next, 100 mL NaOH 50% was added to the powder, heated at 60 °C, and stirred with a magnetic stirrer for 5 h. The powder was washed using distilled

water several times until reaching its neutral condition. The product was finally calcined at 750 °C for 3 h.

Preparation of hydroxyapatite/MnFe₂O₄ composite

The synthesis of hydroxyapatite/MnFe₂O₄ composite was carried out by the co-precipitation method. The mass ratio of hydroxyapatite and MnFe₂O₄ was 1:1. Hydroxyapatite of 11.53 g was added to a 200 mL solution of 0.05 mol manganese(II) chloride and 0.1 mol iron(III) chloride at room temperature. The mixture was stirred and added by 3 M NaOH solution gradually until reaching a pH of 11. The product was washed with distilled water until reaching a neutral pH and then calcined at 600 °C for 1 h at 10 °C/min heating rate.

Determination of pHPZC

The pH change at the point of zero charges (pH$_{PZC}$) was determined by adding 0.25 g of hydroxyapatite/MnFe₂O₄ composite into 50 mL of 0.1 M KNO₃ solution. Sequentially, a pH ranging from 2 to 10 was set up using 1 M HCl and 1 M NaOH solutions. Next, each of the solutions obtained was stirred at 120 rpm for 24 h at room temperature. The final pH values were measured using a pH meter.

Batch adsorption study

The adsorption of Cd(II) and Ni(II) ions was processed in a batch experiment under the effects of pH solution, initial concentration, and contact time. The pH solution effect was observed in 250 mL conical flasks containing 0.1 g of the composite and 100 mL of Cd(II) and Ni(II) ions solution with a concentration of 10 mg/L. Variations in pH of solutions made from 2 to 8 were adjusted by adding HCl 1 M and NaOH 1 M solutions. The solutions were stirred using a shaker at 200 rpm for 60 min. After the adsorption, the concentration of Cd(II) and Ni(II) ions in each solution was determined by AAS. The effect of the initial concentration was evaluated on the concentration variations of 10–80 mg/L. Meanwhile, the contact time was evaluated from 10 to 150 min. All experiments were carried out in triplicate, and the mean values were used for data analysis.

Desorption process

In the batch desorption method, the hydroxyapatite/MnFe₂O₄ composite was reused to adsorb Cd(II) and Ni(II) ions. Desorption of Cd(II) and Ni(II) ions from hydroxyapatite/MnFe₂O₄ composite was studied using 1 M NaCl solution and 0.1 M EDTA [1]. A total of 100 mL of the desorbing eluent was poured into a 250 mL Erlenmeyer containing 0.1 g of the composite, which had absorbed Cd(II) and Ni(II) ions with an initial concentration of 60 mg/L. The desorption process was carried out using a shaker for 3 h at room temperature. The Cd(II) and Ni(II) ions desorbed concentrations were determined using AAS.

■ RESULTS AND DISCUSSION

Characteristic of Hydroxyapatite/MnFe₂O₄ Composite

XRD pattern was used to identify the purity and crystallinity of the adsorbent. The XRD patterns of hydroxyapatite and hydroxyapatite/MnFe₂O₄ composite are shown in Fig. 1. The figure shows that the diffractogram of hydroxyapatite/MnFe₂O₄ is more amorphous than hydroxyapatite because MnFe₂O₄ is more amorphous than hydroxyapatite. The characteristics of the snakehead fish bone-based hydroxyapatite peaks are per JCPDS No. 09-0432. The peaks appear at 2θ = 25.78°, 31.72°, 32.06°, 32.40°, 46.02°, and 49.48°, in accordance with 2θ of JCPDS, namely at 25.879° (002), 31.773° (211), 32.196° (112), 32.902° (300), 46.711° (222), and 49.648° (213). Therefore, hydroxyapatite has a hexagonal crystal structure. The peaks of hydroxyapatite/MnFe₂O₄ composite were overlapping
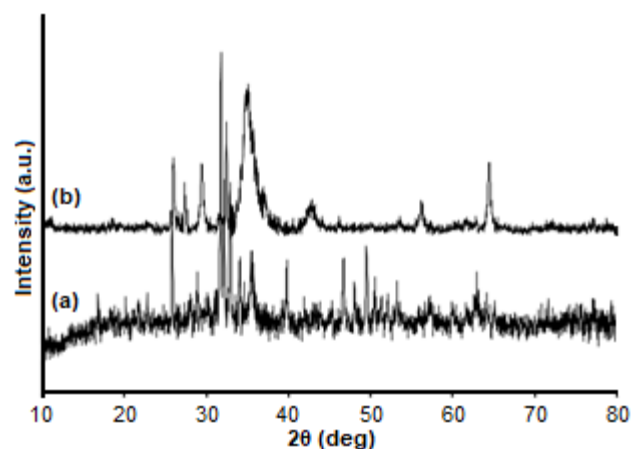

Fig 1. XRD patterns for the (a) hydroxyapatite and (b) hydroxyapatite/MnFe₂O₄ composite

1474

Indones. J. Chem., 2021, 21 (6), 1471 - 1483

hydroxyapatite and $MnFe_2O_4$, the latter of which appeared at 2θ = 18.72°, 29.54°, 35.0°, 43.12°, 53.74°, 56.22°, and 64.54°, indicating the *hkl* plane, namely (111), (220), (311), (400), (422), (511), and (440), following JCPDS 74-2403. Based on these peaks, it can be confirmed that $MnFe_2O_4$ has a face-centered cubic structure with a lattice constant of 8.470 Å.

Fig. 2 shows the FTIR spectra of hydroxyapatite and hydroxyapatite/$MnFe_2O_4$ composite. The wavenumbers at 3418 and 1626 cm^{-1} appear on hydroxyapatite are O–H stretching vibrations and indicating the adsorption of water molecules. Wavenumbers at 3416 and 1628 cm^{-1} also appear in hydroxyapatite/$MnFe_2O_4$ composite. Stretching vibrations of P–O bonds are shown at wavenumbers of 567, 602, 964, and 1036 cm^{-1} in hydroxyapatite, and at 565, 601.7, 962, and 1038 cm^{-1} in hydroxyapatite/$MnFe_2O_4$ composite. The wavenumber corresponds to the tetrahedral PO_4^{3-} vibration [31]. The CO_3^{2-} groups can be identified at wavenumbers of around 870 and 1402–1460 cm^{-1} [32]. In hydroxyapatite, the CO_3^{2-} group appears at 876 and 1414 cm^{-1}, whereas hydroxyapatite/$MnFe_2O_4$ composite is at 870 and 1404 cm^{-1}. These groups come from fish bones that remain in the extraction process. The presence of CO_2 in hydroxyapatite and hydroxyapatite/$MnFe_2O_4$ composite comes from the air can be identified at wavenumbers 2365 and 2369 cm^{-1}. The main peak in wavenumbers below 1000 cm^{-1} in the hydroxyapatite/$MnFe_2O_4$ composite indicates the presence of ferrites [29]. Stretching vibrations at 471 and 604 cm^{-1} show the formation of the spinel ferrite structure. The absorption band at wavenumber 565 cm^{-1} reflects manganese ferrite's intrinsic vibration, which peak overlaps with stretching P–O vibrations.

FTIR spectra of hydroxyapatite/$MnFe_2O_4$ composite after adsorbing Ni(II) and Cd(II) showed a shift in wavenumbers. The shifted wavenumbers are 3416, 1628, 1404, 1038, 962, and 565 cm^{-1}. After Ni(II) adsorption, they shifted to 3412, 1584, 1433, 990, 920, 561, and 525 cm^{-1}, while after Cd(II) adsorption, they were observed at 3385, 1603, 1435, 1013, 930, 570, and 534 cm^{-1}. The peak shifts to the lower frequencies indicate that the formation of composite bonds with Ni(II) and Cd(II) requires less energy for vibration [33].

Fig. 3 shows the surface morphology of hydroxyapatite and hydroxyapatite/$MnFe_2O_4$ composite. No significant change in the surface morphology of hydroxyapatite after the composite was formed occurred, but the composite surface appeared to be more
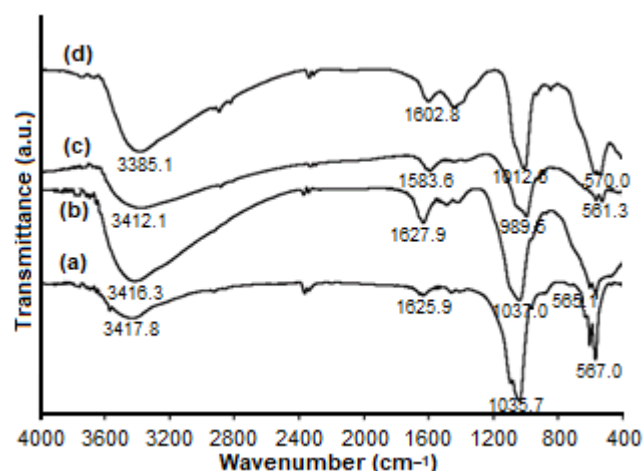
Fig 2. FTIR spectra of (a) hydroxyapatite and (b) hydroxyapatite/$MnFe_2O_4$ composite (c) hydroxyapatite/$MnFe_2O_4$ composite after Ni(II) adsorption and (d) hydroxyapatite/$MnFe_2O_4$ composite after Cd(II) adsorption
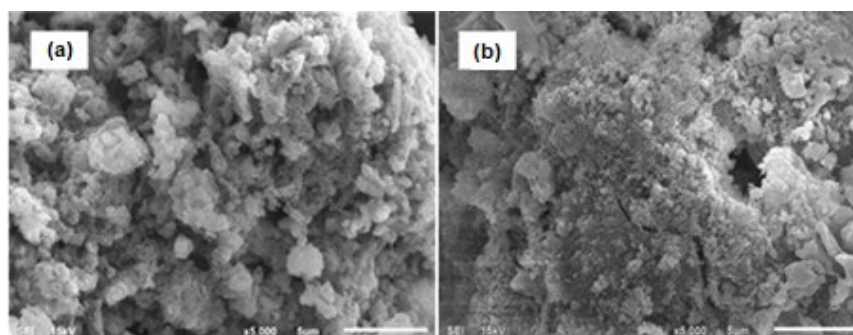
Fig 3. SEM image (5000×) of (a) hydroxyapatite and (b) hydroxyapatite/$MnFe_2O_4$ composite

compact than hydroxyapatite. $MnFe_2O_4$ is deposited randomly on the hydroxyapatite surface. Table 1 shows the composition of the hydroxyapatite and hydroxyapatite/$MnFe_2O_4$ composite due to EDX analysis. In this research, the Ca/P molar ratio of hydroxyapatite was 1.65, close to the theoretical value, i.e., 1.67. The presence of Mn in the composite shows that the process of forming the composite succeed.

The magnetic properties of hydroxyapatite/$MnFe_2O_4$ composite were determined by using VSM at room temperature. Hysteresis curves show the magnetic behavior of a material. Fig. 4 shows the saturation magnetization of hydroxyapatite/$MnFe_2O_4$ composite, which is super magnetic with a saturation magnetization of 21.95 emu/g. Another study reported that the synthesize of $MnFe_2O_4$-activated carbon composite had a saturation magnetization of 17.91 emu/g [34]. Thus, the saturation magnetization value of the $MnFe_2O_4$-activated carbon composite is smaller than the pure $MnFe_2O_4$.

Table 2 presents the BET surface area, mean pore diameter, and pore volume of the samples. It was found that the surface area of hydroxyapatite/$MnFe_2O_4$ composite is more diminutive than hydroxyapatite. The presence of $MnFe_2O_4$ partially fills the pores of hydroxyapatite; hence the surface area is reduced. The hydroxyapatite/$MnFe_2O_4$ composite has a mean pore diameter larger than hydroxyapatite. $MnFe_2O_4$ particles possibly underwent agglomeration and are positioned on the surface of the hydroxyapatite, which causes an increase in the mean pore diameter [35]. The same phenomenon was reported in $MnFe_2O_4$-activated carbon composites [29]. The presence of ferrite compounds causes the surface area to decrease, and the mean pore diameter increases.

The pH value at the zero charge (pH_{PZC}) is one of the adsorbent characteristics affecting adsorption capacity.

The pH_{PZC} value provides information about the nature of the hydroxyapatite/$MnFe_2O_4$ composite surface charge. Under the condition of pH solution < pH_{PZC}, the composite surface is positively charged, and conversely, it is negatively charged if the pH of the solution > pH_{PZC} [36]. In this study, the pH_{PZC} of hydroxyapatite/$MnFe_2O_4$ composite was 5.8 (Fig. 5).

Batch Sorption

The batch adsorption method was used to study the adsorption properties of hydroxyapatite/$MnFe_2O_4$ composite against Cd(II) and Ni(II) ions. This research
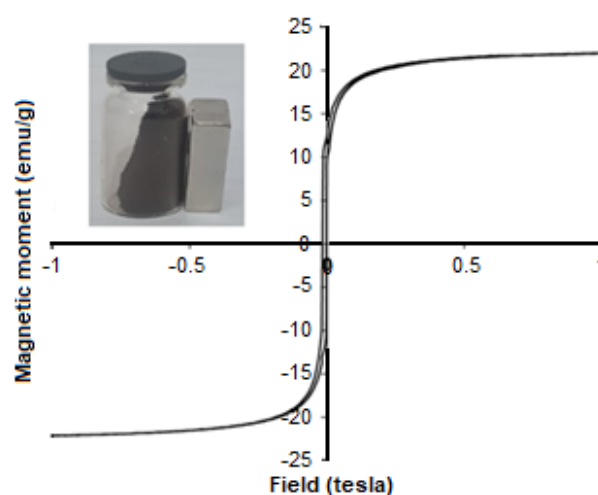

Fig 4. Magnetic saturation of hydroxyapatite/$MnFe_2O_4$ composite

Table 1. Element composition of hydroxyapatite and hydroxyapatite/$MnFe_2O_4$ composite

Element	Percentage (%)	
	Hydroxyapatite	Composite
P	18.72	9.12
O	41.35	36.42
Ca	39.93	19.20
Mn	-	11.06
Fe	-	24.20

Table 2. Characteristic of hydroxyapatite and hydroxyapatite/$MnFe_2O_4$ composite using the BET method

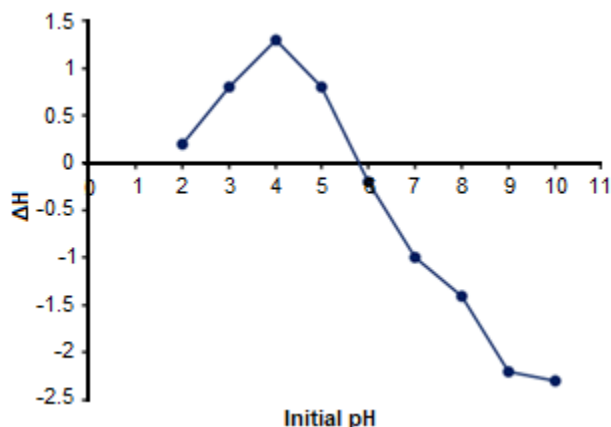| Characteristic	Hydroxyapatite	Hydroxyapatite/$MnFe_2O_4$ composite
BET surface area (m²/g)	110.5	97.8
Average pore diameter (nm)	7.92	10.52
Pore volume (cm³/g)	0.41	0.32

Fig 5. pH_{PZC} of hydroxyapatite/MnFe$_2$O$_4$ composite

studied the influence of pH, contact time, and initial concentration on the adsorption capacity of hydroxyapatite/MnFe$_2$O$_4$ composites. pH is one of the essential variables in the adsorption process. The adsorption mechanism depends on the pH of the solution, which affects the degree of ionization, the adsorbent surface charge, and the adsorbate speciation [1].

Adsorption of Cd(II) and Ni(II) ions by hydroxyapatite/MnFe$_2$O$_4$ composites was carried out in the pH range of 2–8 (Fig. 6). The concentration of Cd(II) and Ni(II) ions was 10 mg/L in 100 mL, the amount of hydroxyapatite/MnFe$_2$O$_4$ composites was 0.1 g. Therefore, the optimum pH was 6 for Cd(II) and Ni(II) ions. Under the condition of pH < pH_{PZC}, the hydroxyapatite/MnFe$_2$O$_4$ composite was negatively charged, so competition occurred between H$^+$ ions and
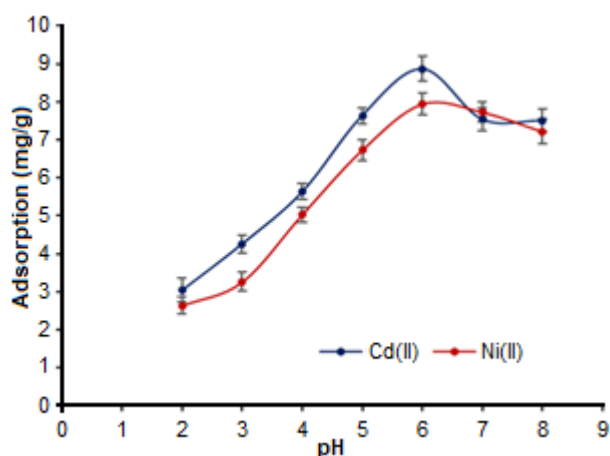
metal ions. Consequently, the adsorption capacity decreased. Under the condition of pH > pH_{PZC}, the hydroxyapatite/MnFe$_2$O$_4$ composite has a negative charge resulting in electrostatic attraction with positively charged Cd(II) and Ni(II) ions, thus increasing the adsorption capacity. Another author reported the same results that the optimum pH of the adsorption of Cu(II) and Cd(II) ions using Fe$_3$O$_4$/hydroxyapatite/β-cyclodextrin composite is 6, where the pH_{PZC} adsorbent was 5 [26]. At pH above 7, Cd(II) and Ni(II) ions bind to hydroxide and form precipitate [14].

The effects of the initial concentration of Cd(II) and Ni(II) ions on the adsorption capacity of hydroxyapatite/MnFe$_2$O$_4$ composites are depicted in Fig. 7. The adsorption process was carried out with adsorbent weight 0.1 g, solution volume of 100 mL, pH 6, and contact time of 60 min. As the concentration of Cd(II) and Ni(II) ions increases, the more significant number of Cd(II) and Ni(II) ions is being adsorbed by hydroxyapatite/MnFe$_2$O$_4$ composite. Interactions between metal ions and hydroxyapatite/MnFe$_2$O$_4$ composite occurred due to electrostatic interactions and ion exchange. The Ca(II) ions in hydroxyapatite can be replaced by metal ions(M) according to the following reaction [20,25].

$$Ca_{10}(PO_4)_6(OH)_2 + xM^{2+} \rightarrow Ca_{10-x}M_x(PO_4)_6(OH)_2 + xCa^{2+} \quad (1)$$

Fig 6. Effect of pH solution on the adsorption of Cd(II) and Ni(II) ions by hydroxyapatite/MnFe$_2$O$_4$ composite
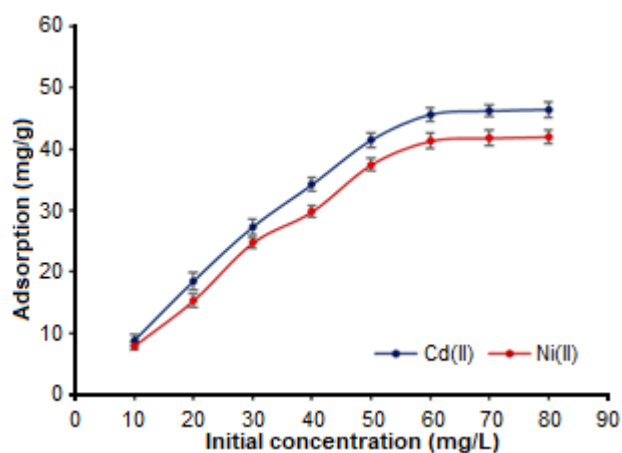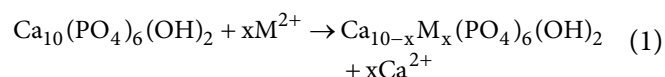

Fig 7. Effect of initial concentration on the adsorption of Cd(II) and Ni(II) ions by hydroxyapatite/MnFe$_2$O$_4$ composite

The contact time effect was evaluated under experiment conditions as follows: 0.1 g of hydroxyapatite/$MnFe_2O_4$ composite, 100 mL of Cd(II) and Ni(II) ions with a concentration of 60 mg/L, solution pH of 6, room temperature with a contact time of 10–150 min. Fig. 8 shows that the amount of Cd(II) and Ni(II) ions adsorbed is proportional to the contact time until equilibrium is achieved. Optimum contact times for Cd(II) and Ni(II) ions were obtained at 90 and 100 min, respectively.

Adsorption Kinetics

Adsorption kinetics study provides information about optimum conditions, mechanism of sorption, and possible rate-controlling step. In this study, the kinetics of Cd(II) and Ni(II) adsorption by hydroxyapatite/$MnFe_2O_4$ were evaluated based on two models, namely the pseudo-first-order and pseudo-second-order models. The model uses equations as follows [30]:

$$\log(q_e - q_t) = \log q_e - \frac{k_1}{2.303} \tag{2}$$

$$\frac{t}{q_t} = \frac{1}{k_2 q_e^2} + \frac{t}{q_e} \tag{3}$$

where q_e (mg/g) is the adsorption capacity at equilibrium, q_t (mg/g) is the adsorption capacity at time t (min), and k_1 (1/min) and k_2 (g/mg/min) are the pseudo-first-order and pseudo-second-order constants, respectively.

Fig. 9 shows the graphs of the pseudo-first-order and pseudo-second-order adsorption kinetics of Cd(II) and Ni(II) ions by hydroxyapatite/$MnFe_2O_4$ composite. The correlation coefficient (R^2) value of the pseudo-first-order is lower than the pseudo-second-order for both Cd(II) and Ni(II) ions. However, R^2 for the pseudo-second-order is closer to 1 ($R^2 > 0.995$), indicating that the adsorption kinetics that is suitable for describing the adsorption of Cd(II) and Ni(II) ions by hydroxyapatite/$MnFe_2O_4$ composite is the pseudo-second-order.

Table 3 shows the kinetics parameters of the adsorption of Cd(II) and Ni(II) ions by hydroxyapatite/$MnFe_2O_4$ composite. The values of k_1 and k_2 for Cd(II) ions were lower than those of Ni(II) ions, indicating that Cd(II) ions were adsorbed more
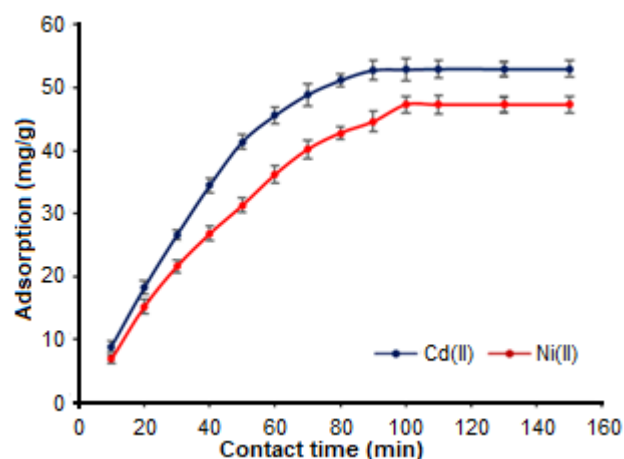
Fig 8. Effect of contact time on the adsorption of Cd(II) and Ni(II) ions by hydroxyapatite/$MnFe_2O_4$ composite
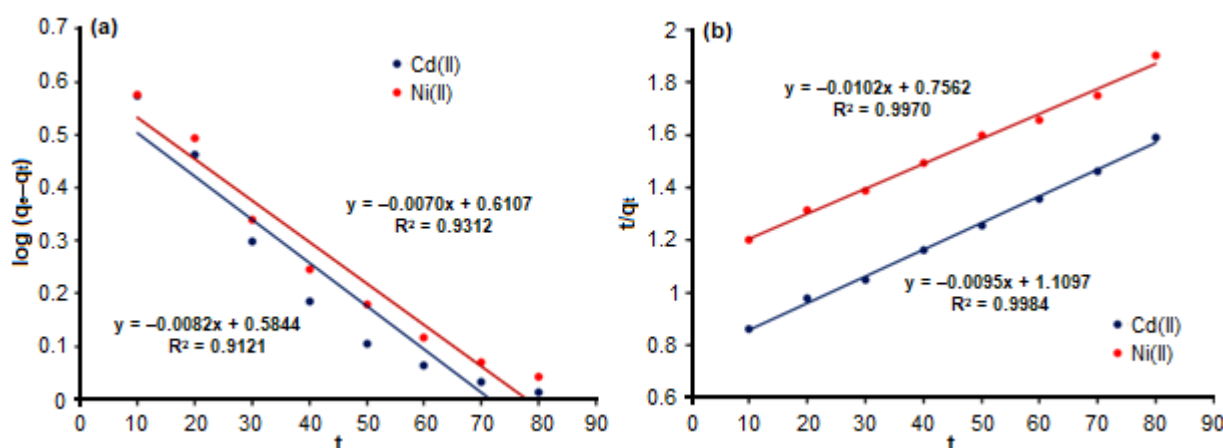
Fig 9. Pseudo- (a) first-order and (b) second-order kinetics of adsorption of Cd(II) and Ni(II) ions by hydroxyapatite/$MnFe_2O_4$ composite

Table 3. Parameters of kinetics for adsorption of Cd(II) and Ni(II) ions by hydroxyapatite/MnFe$_2$O$_4$ composite

Parameters	Metal ions	
	Cd(II)	Ni(II)
Pseudo-first order		
R^2	0.9121	0.9312
k_1 (1/min)	0.00351	0.00304
q_e (mg/g)	3.841	3.838
Pseudo-second order		
R^2	0.9984	0.9970
k_2 (g/mg min)	8.1×10^{-5}	13.7×10^{-5}
q_e (mg/g)	105.263	98.038

quickly by hydroxyapatite/MnFe$_2$O$_4$ composite than Ni(II) ions. Furthermore, the q_e value of Cd(II) ions is higher than that of Ni(II) ions in the pseudo-first-order and pseudo-second-order. However, other studies reported the adsorption of heavy metal ions followed pseudo-second-order, i.e., Cd(II) and Ni(II) ions studied using expanded perlite [12] and succinylated hay [15].

Isotherm of Adsorption

Two models of adsorption isotherm often used are Langmuir and Freundlich's isotherm models. The Langmuir isotherm model assumes monolayer adsorption, in which the adsorption occurs in a limited number and the active sites are localized and identical. Meanwhile, the Freundlich isotherm model describes a multilayer isotherm model with a heterogeneous surface and non-uniform heat distribution. Furthermore, the

adsorption energy decreases exponentially after the adsorption process [3]. The equation that describes both the Langmuir and Freundlich isotherm models is as follows:

$$\frac{C_e}{q_e} = \frac{1}{K_L q_{max}} + \frac{C_e}{q_{max}} \quad (4)$$

$$\log q_e = \log K_f + \frac{1}{n} \log C_e \quad (5)$$

where C_e (mg/L) is the concentration of metal ions at equilibrium, q_e (mg/g) is the amount of metal ions adsorbed at equilibrium, q_{max} (mg/g) is the maximum number of metal ions absorbed per mass of adsorbent, and K_L (L/g) is the adsorption equilibrium constant. K_f (mg/g(mg/L)$^{1/n}$ is the constant fo Freundlich and $\frac{1}{n}$ is the adsorption intensity.

Fig. 10 shows the Langmuir and Freundlich isotherm adsorption models of Cd(II) and Ni(II) ions by hydroxyapatite/MnFe$_2$O$_4$ composite. The adsorption parameters are presented in Table 4. The adsorption of Cd(II) and Ni(II) ions follows the Langmuir isotherm model. The correlation coefficient (R^2) of the Langmuir isotherm model was more significant than the Freundlich isotherm model. The Langmuir isotherm also indicates that there is no interaction between adsorbates [26].

R_L is defined as a separation factor, and an essential parameter in the Langmuir isotherm used to determine the favorableness of the adsorption processes. If the value of $R_L > 1$, then the adsorption process is unfavorable,
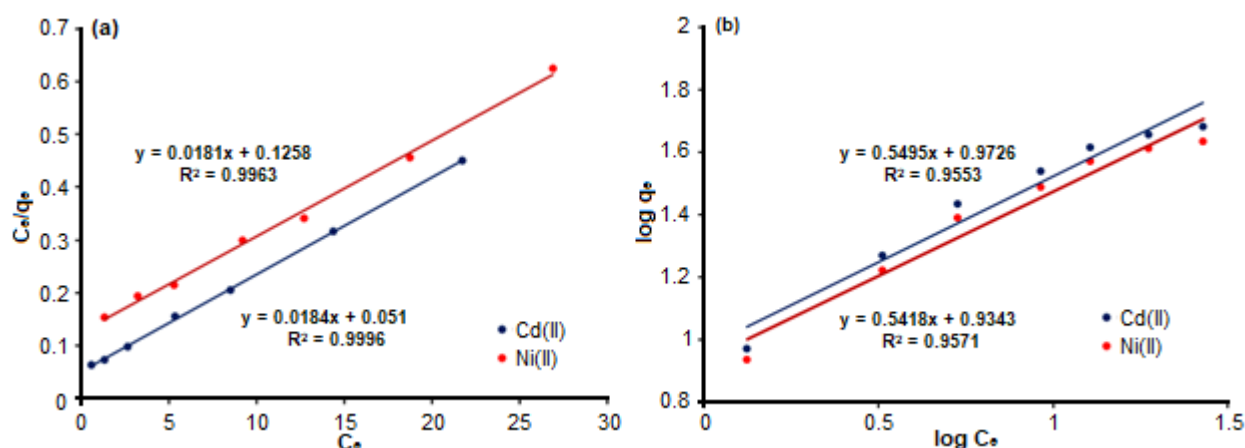

Fig 10. (a) Langmuir dan (b) Freundlich isotherm models adsorption of Cd(II) and Ni(II) ions by hydroxyapatite/MnFe$_2$O$_4$ composite

Table 4. Parameters of isotherm for adsorption of Cd(II) and Ni(II) ions by hydroxyapatite/$MnFe_2O_4$ composite

Parameters	Metal ions	
	Cd(II)	Ni(II)
Langmuir isotherm		
R^2	0.9996	0.9963
K_L (L/g)	0.3608	0.1677
q_{max} (mg/g)	54.348	47.393
Freundlich isotherm		
R^2	0.9553	0.9751
K_f (mg/g(mg/L)$^{1/n}$)	9.36	8.02
n	1.819	1.678
q_{exp} (mg/g)	52.810	47.330

while if $R_L < 1$, then the process is favorable. The value R_L is determined based on the following equation:

$$R_L = \frac{1}{\left(1 + K_L C_0\right)} \tag{6}$$

C_0 (mg/L) is the initial concentration. The results show that the R_L values for various initial concentrations are between $0 < R_L < 1$. These findings indicate that the adsorption processes are favorable. These results were also confirmed by the values of n, which were n > 1, indicating that the adsorption process is favorable. The n values for the adsorption of Cd(II) and Ni(II) ions are 1.819 and 1.678, respectively.

The adsorption capacity data results showed that the calculated adsorption capacity (q_{max}) was greater than that of the experiment (q_{exp}) for both metal ions. The maximum adsorption capacity of hydroxyapatite/$MnFe_2O_4$ composite for Cd(II) ions is 54.3 mg/g greater than Ni(II) ions, 47.3 mg/g. The effectivity of adsorption depends on the size of the ions in solution, ionic radius, and atomic mass [37]. The ionic radius of Cd(II) (109 pm) is greater than Ni(II) (83 pm), so it is reasonable that the adsorption capacity of hydroxyapatite/$MnFe_2O_4$ composite for Cd(II) ions is greater [1]. The other research reported that the selectivity of metal ions against calcium alginate is Pb > Cu > Cd > Ni > Zn > Co, based on equilibrium constant (K). K_{Cd} value (172 kg L/mol^2) is greater than K_{Ni} (30.8 kg L/mol^2) [38]. Table 5 shows the adsorption capacities of several adsorbents against Cd(II) and Ni(II) ions. The adsorption capacity of hydroxyapatite/$MnFe_2O_4$ composites is greater than other adsorbents.

Desorption

In this study, hydroxyapatite/$MnFe_2O_4$ composite regeneration was carried out using two eluents, namely NaCl (inorganic eluent) and EDTA (organic eluent) solutions. Cd(II) and Ni(II) ions from hydroxyapatite/$MnFe_2O_4$ composite desorbed easier when using NaCl compared to EDTA (Fig. 11). The desorption mechanism using NaCl involved electrostatic attraction or ion exchange, whereas when desorption is using EDTA, it occurs due to the chemical bond formed by the chelating agent [1].

Table 5. The adsorption capacity of several adsorbents against Cd(II) and Ni(II) ions at room temperature

| Sorbent	pH	Adsorption capacity (mg/g)		Reference
		Cd(II)	Ni(II)	
Expanded perlite	6	1.791	2.24	[13]
Chitosan-Methylmethacrylic acid	5	2.42	1.13	[1]
Bottlebrush seeds	6	39.525	-	[39]
Ag-$MnFe_2O_4$-bentonite	6	48.31	-	[2]
Green longan hull	5	4.19	3.96	[14]
Calcium alginate beads (CA)	6	38.049	14.668	[3]
Spent coffee ground (SCGs)	6	10.671	5.608	[3]
CA-SCGs	6	25.495	12.320	[3]
Graphite decorated manganese oxide	5		0.110	[30]
Callinectes sapidus biomass	6	29.23	29.15	[40]
Sludge	5	1.53	-	[41]
Hydroxyapatite/$MnFe_2O_4$ composite	6	54.348	47.393	In this study
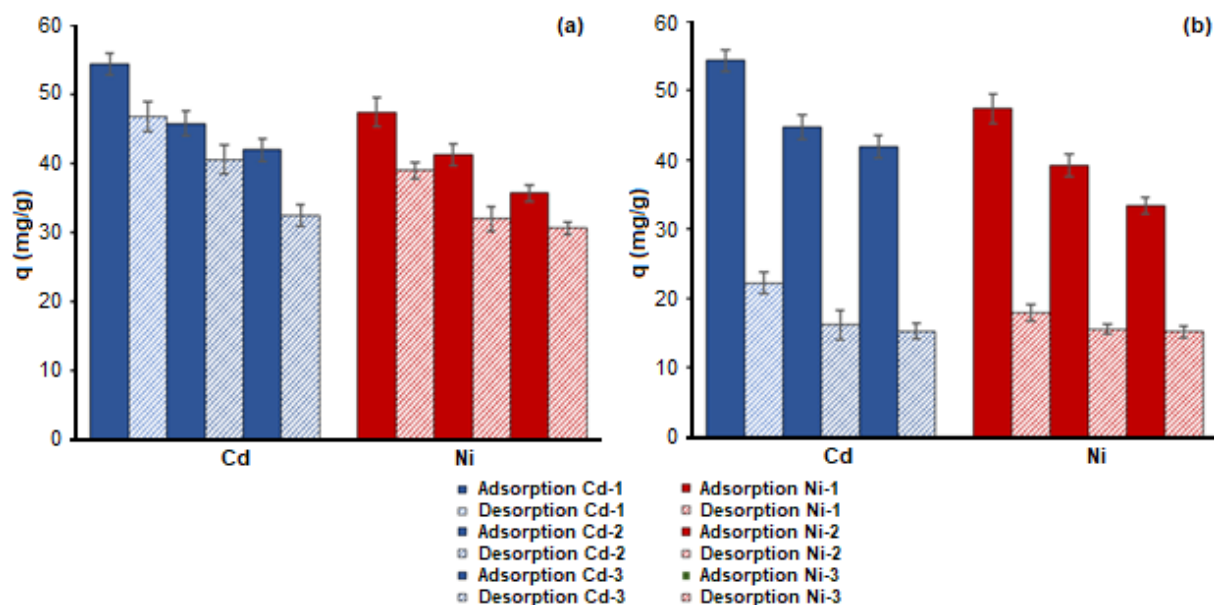
Fig 11. Adsorption-desorption of Cd(II) and Ni(II) ions using eluents (a) NaCl and (b) EDTA

Other studies on the desorption of Cd(II) and Pb(II) ions from $MnFe_2O_4$-graphene showed that desorption occurred electrostatically using HCl as an eluent [42]. The percentage of desorption depends on the type of metal ions and eluents used [25]. Desorption of Cu(II), Pb(II), and Cd(II) ions adsorbed by spent-coffee-grounds shows different results, i.e., citric acid is effective for desorption of Cu(II) ions, calcium chloride is effective for desorption of Pb(II) ions, and HNO_3 can properly desorb these three metal ions.

■ **CONCLUSION**

Hydroxyapatite/$MnFe_2O_4$ composite having magnetic properties was successfully synthesized to adsorb Cd(II) and Ni(II) ions from solutions. The optimum adsorption process for Cd(II) ions occurs at pH of 6, initial concentration of 60 mg/L, and contact time of 90 min, while Ni(II) ions adsorbed optimally at a pH of 6, initial concentration of 60 mg/L, and contact time of 100 min. The pseudo-second-order adsorption kinetics best suit for describing the adsorption kinetics of Cd(II) and Ni(II) ions by hydroxyapatite/$MnFe_2O_4$ composite. The adsorption capacity of hydroxyapatite/$MnFe_2O_4$ composite for Cd(II) ion (54.348 mg/g) is more significant than Ni(II) ion (47.393 mg/g). The Cd(II) and

Ni(II) ions can be desorbed from hydroxyapatite/$MnFe_2O_4$ composite using NaCl and EDTA, provided that NaCl is a better eluent than EDTA. It can be suggested that hydroxyapatite/$MnFe_2O_4$ composite can reduce pollutants, primarily metal ions, in solutions. Hydroxyapatite/$MnFe_2O_4$ composite has magnetic properties; hence the adsorbent can be separated simply by using an external magnet.

■ **AUTHOR CONTRIBUTIONS**

Poedji Loekitowati Hariani, Muhammad Said, Addy Rachmat, and Salni carried out the experiment. Poedji Loekitowati Hariani and Muhammad Said contributed to the synthesis and characterization of materials, Addy Rachmat and Salni contributed to adsorption and desorption data interpretation. Finally, all the authors discuss and contribute to the final manuscript.

Indones. J. Chem., 2021, 21 (6), 1471 - 1483

1481

■ REFERENCES

[1] Heidari, A., Younesi, H., Mehraban, Z., and Heikkinen, H., 2013, Selective adsorption of Pb(II), Cd(II), and Ni(II) ions from aqueous solution using chitosan-MAA nanoparticles, *Int. J. Biol. Macromol.*, 61, 251–263.

[2] Li, Q., Zhao, Y., Qu, D., Wang, H., Chen, J., and Zhou, R., 2018, Preparation of Ag-MnFe$_2$O$_4$-bentonite magnetic composite for Pb(II)/Cd(II) adsorption removal and bacterial inactivation in wastewater, *Chem. Res. Chin. Univ.*, 34 (5), 808–816.

[3] Torres-Caban, R., Vega-Olivencia, C.A., and Mina-Camilde, N., 2019, Adsorption of Ni^{2+} and Cd^{2+} from water by calcium alginate/spent coffee grounds composite beads, *Appl. Sci.*, 9 (21), 4531.

[4] Liao, V.H.C., Chien, M.T., Tseng, Y.Y., and Qu, K.L., 2006, Assessment of heavy metal bioavailability in contaminated sediments and soils green fluorescent protein-based bacterial biosensors, *Environ. Pollut.*, 142 (1), 17–23.

[5] Soylak, M., Kars, A., and Narin, I., 2008, Coprecitation of Ni^{2+}, Cd^{2+} and Pb^{2+} for preconcentration in environmental samples prior to flame atomic absorption spectrometric determination, *J. Hazard. Mater.*, 159 (2-3), 435–439.

[6] Kasprzak, K.S., Sunderman Jr., F.W., and Salnikow, K., 2003, Nickel carcinogenesis, *Mutat. Res., Fundam. Mol. Mech. Mutagen.*, 533 (1-2), 67–97.

[7] Sobhanardakani, S., and Zandipak, R., 2015, Adsorption of Ni(II) and Cd(II) from aqueous solutions using modified rice husk, *Iran. J. Health Sci.*, 3 (1), 1–9.

[8] Qdais, H.A., and Moussa, H., 2004, Removal of heavy metals from wastewater by membrane processes: A comparative study, *Desalination*, 164 (2), 105–110.

[9] Igiri, B.E., Okoduwa, S.I.R., Idoko, G.O., Akabuogu, E.P., Adeyi, A.O., and Ejiogu, I.K., 2018, Toxicity and bioremediation of heavy metals contaminated ecosystem from tannery wastewater: A review, *J Toxicol.*, 2018, 2568038.

[10] Thaçi, B.S., and Gashi, S.T., 2019, Reverse osmosis removal of heavy metals from wastewater effluents using biowaste materials pretreatment, *Pol. J. Environ. Stud.*, 28 (1), 337–341.

[11] Zewail, T.M., and Yousef, N.S., 2015, Kinetic study of heavy metal ions removal by ion exchange in batch conical air spouted bed, *Alexandria Eng. J.*, 54 (1), 83–90.

[12] Torab-Mostaedi, M., Ghassabzadeh, H., Ghannadi-Maragheh, M., Ahmadi, S.J., and Taheri, H., 2010, Removal of cadmium and nickel from aqueous solution using expanded perlite, *Braz. J. Chem. Eng.*, 27 (2), 299–308.

[13] Wijesinghe, W.P.S.L., Mantilaka, M.M.M.G.P.G., Peiris, T.A.N., Rajapakse, R.M.G., Wijayantha, K.G.U., Pitawala, H.M.T.G.A., Premachandra, T.N., Herath, H.M.T.U., and Rajapakse, R.P.V.J., 2018, Preparation and characterization of mesoporous hydroxyapatite with non cytotoxicity and heavy metal adsorption capacity, *New J. Chem.*, 42 (12), 10271–10278.

[14] Guo, X., Tang, S., Song, Y., and Nan, J., 2018, Adsorptive removal of Ni^{2+} and Cd^{2+} from wastewater using a green longan hull adsorbent, *Adsorpt. Sci. Technol.*, 36 (1-2), 762–773.

[15] Lin, P., Wu, J., Ahn, J., and Lee, J., 2019, Adsorption characteristic of Cd(II) and Ni(II) from aqueous solution using succinylated hay, *Int. J. Miner. Metall. Mater.*, 26 (10), 1239–1246.

[16] Roy, S., and Das, P., 2016, Thermodynamic and kinetics study of de-fluoridation in wastewater using hydroxyapatite (Hap) as adsorbent: optimization using response surface methodology, *Front. Nanosci. Nanotechnol.*, 2 (3), 121–128.

[17] Hamzah, S., Yatim, N.I., Alias, M., Ali, A., Rasit, N., and Abuhabib, A., 2019. Extraction of hydroxyapatite from fish scales and its integration with rice husk for ammonia removal in aquaculture wastewater, *Indones. J. Chem.*, 19 (4), 1019–1030.

[18] Iconaru, S.L., Heino, M.M., Guegan, R., Beuran, M., Costecu, A., and Predoi, D., 2018, Adsorption of Pb(II) ions onto hydroxyapatite nanopowders in aqueous solution, *Materials*, 11 (11), 2204.

[19] Le, D.T., Le, T.P.T., Do, H.T., Vo, H.T., Pham, N.T., Nguyen, T.T., Cao, H.T., Nguyen, P.T., Dinh, T.M.T., Le, H.V., and Tran, D.L., 2019, Fabrication

of porous hydroxyapatite granules as an effective adsorbent for the removal of aqueous Pb(II) ions, *J. Chem.*, 2019, 8620181.

[20] Dabiri, S.M.H., Rezaie, A.A., Moghimi, M., and Rezaie, H., 2018, Extraction of hydroxyapatite from fishbone and its application, *BioNanoScience*, 8 (3), 823–834.

[21] Idea, P., Degli Esposti, L., Miguel, C.C., Adamiano, A., Iafisco, M., and Castilho, P.C., 2021, Extraction and characterization of hydroxyapatite-based materials from grey triggerfish skin and black scabbardfish bones, *Int. J. Appl. Ceram. Technol.*, 18 (1), 235–243.

[22] Zairin, D.A., and Phang, S.W., 2018, Calcination time and temperature effect on natural hydroxyapatite obtained from fish bones for bone tissue engineering, *Int. J. Eng. Sci. Technol.*, Special issue August, 39–51.

[23] Hariani, P.L., Muryati, M., and Said, M., 2019, Kinetic and thermodynamic adsorption of nickel(II) onto hydroxyapatite prepared from Snakehead (*Channa striata*) fish bone, *Mediterr. J. Chem.*, 9 (2), 85–94.

[24] Hariani, P.L., Muryati, M., Said, M., and Salni, S., 2020, Synthesis of nano-hydroxyapatite from Snakehead (*Channa striata*) fish bone and its antibacterial properties, *Key Eng. Mater.*, 840, 293–299.

[25] Dong, L., Zhu, Z., Qiu, Y., and Zhao, Z., 2010, Removal of lead from aqueous solution by hydroxyapatite/magnetite composite adsorbent, *Chem. Eng. J.*, 165 (3), 827–834.

[26] Ansari, A., Vahedi. S., Tavakoli, O., Khoobi, M., and Faramarzi, M.A., 2018, Novel Fe_3O_4/hydroxyapatite/ β-cyclodextrin nanocomposite adsorbent: synthesis and application in heavy metal removal from aqueous solution, *Appl. Organomet. Chem.*, 33 (1), e4634.

[27] Ragab, A., Ahmed, I., and Bader, D., 2019, The removal of brilliant green dye from aqueous solution using hydroxyapatite/chitosan composite as sorbent, *Molecules*, 24 (5), 847.

[28] Shao, L., Ren, Z., Zhang, G., and Chen, L., 2012, Facile synthesis, characterization of a $MnFe_2O_4$/ activated carbon magnetic composite and its effectiveness in tetracycline removal, *Mater. Chem. Phys.*, 135 (1), 16–24.

[29] Podder, M.S., and Majumder, C.B., 2016, Studies on the removal of As(III) and As(V) through their adsorption onto granular activated carbon/ $MnFe_2O_4$ composite: Isotherm studies and error analysis, *Compos. Interfaces*, 23 (4), 327–372.

[30] Do, Q.C., Choi, S., Kim, H., and Kang, S., 2019, Adsorption of lead and nickel on to expanded graphite decorated with manganese oxide nanoparticles, *Appl. Sci.*, 9 (24), 5375.

[31] Soejoko, D.S., and Tjia, M.O., 2002, Infrared spectroscopy and X-ray diffraction study on the morphological variations of carbonate and phosphate compounds in giant prawn (*Macrobrachium rosenbergii*) skeletons during its moulting period, *J. Mater. Sci.*, 38 (9), 2087–2093.

[32] Wang, P., Li, C., Gong, H., Jiang, X., Wang, H., and Li, K., 2013, Effects of synthesis conditions on the morphology of hydroxyapatite nanoparticles produced by wet chemical process, *Powder Technol.*, 203 (2), 315–321.

[33] Yari Moghaddam, N., Lorestani, B., Cheraghi, M., and Jamebozorgi, S, 2019, Adsorption of Cd and Ni from water by graphene oxide and graphene oxide-almond shell composite, *Water Environ. Res.*, 91 (6), 475–482.

[34] Riyanti, F., Hariani, P.L., Purwaningrum, W., Elfita, E., Damarril, S.S., and Amelia, I., 2018, The synthesis of $MnFe_2O_4$-activated carbon composite for removal of methyl red from aqueous solution, *Molekul*, 13 (2), 123–132.

[35] Danmaliki, G.I., and Saleh, T.A., 2016, Influence of conversion parameters of waste tires to activated carbon on adsorption of dibenzothiophene from models fuels, *J. Cleaner Prod.*, 117, 50–55.

[36] Kausar, A., Naeem, K., Hussain, T., Nazli, Z.I.H., Bhatti, H.N., Jubeen, F., Nazir, A., and Iqbal, M., 2019, Preparation and characterization of

chitosan/clay composite for direct rose FRN dye removal from aqueous media: Comparison of linear and non-linear regression methods, *J. Mater. Res. Technol.*, 8 (1), 1161–1174.

[37] Hossain, M.A., Ngo, H.H., Guo, W.S., Nghiem, L.D., Hai, F.I., Vigneswaran, S., and Nguyen, T.V., 2014, Competitive adsorption of metals on cabbage waste from multi-metal solutions, *Bioresour. Technol.*, 160, 79–88.

[38] Jodra, Y., and Mijangos, F., 2001, Ion exchange selectivities of calcium alginate gels for heavy metals, *Water Sci. Technol.*, 43 (2), 237–244.

[39] Rao, R.A.K., and Kashifuddin, M., 2014, Kinetics and isotherm studies of Cd(II) adsorption from aqueous solution utilizing seeds of bottlebrush plant (*Callistemon chisholmii*), *Appl. Water Sci.*, 4 (4), 371–383.

[40] Foroutan, R., Mohammadi, R., Farjadfard, S., Esmaeili, H., Saberi, M., Sahebi, S., Dobaradaran, S., and Ramavandi, B., 2019, Characteristic and performance of Cd, Ini, and Pb bio-adsorption using *Callinectes sapidus* biomass: Real wastewater treatment, *Environ. Sci. Pollut. Res. Int.*, 26, 6336–6347.

[41] Du, X., Cui, S., Fang, X., Wang, Q., and Liu, G., 2020, Adsorption of Cd(II), Cu(II), and Zn(II) by granules prepared using sludge from a drinking water purification plant, *J. Environ. Chem. Eng.*, 8 (6), 104530.

[42] Chella, S., Kollu, P., Komarala, E.V.P.R., Doshi, S., Saranya, M., Felix, S., Ramachandran, R., Saravanan, P., Koneru, V.L., Venugopal, V., Jeong, S.K., and Grace, A.N., 2015, Solvothermal synthesis of MnFe$_2$O$_4$-graphene composite—Investigation of its adsorption and antimicrobial properties, *Appl. Surf. Sci.*, 327, 27–36.